Molybdenum disulfide and water interaction parameters

Mohammad Heiranian,[a] Yanbin Wu,[a] and Narayana R. Aluru[b]
Department of Mechanical Science and Engineering, Beckman Institute for Advanced Science and Technology, University of Illinois at Urbana-Champaign, Urbana, Illinois 61801, USA

(Received 17 April 2017; accepted 23 August 2017; published online 12 September 2017)

Understanding the interaction between water and molybdenum disulfide (MoS_2) is of crucial importance to investigate the physics of various applications involving MoS_2 and water interfaces. An accurate force field is required to describe water and MoS_2 interactions. In this work, water–MoS_2 force field parameters are derived using the high-accuracy random phase approximation (RPA) method and validated by comparing to experiments. The parameters obtained from the RPA method result in water–MoS_2 interface properties (solid-liquid work of adhesion) in good comparison to the experimental measurements. An accurate description of MoS_2-water interaction will facilitate the study of MoS_2 in applications such as DNA sequencing, sea water desalination, and power generation. *Published by AIP Publishing.* [http://dx.doi.org/10.1063/1.5001264]

INTRODUCTION

Water in nanopores and nanochannels has unique properties that differ from those of bulk water.[1,2] These unique properties of confined water can be used to exploit novel functionalities and applications. For example, water in carbon-based nano confinements has been found to possess fast translational motion,[3–7] rotation-translation coupling,[8] and fast rotational motion[9,10] leading to potential applications such as seawater desalination[11,12] and energy storage.[13] Compared to nanoporous graphene and carbon nanotubes, nanopores in molybdenum disulfide (MoS_2) membranes have shown enhanced biological compatibility and higher signal-to-noise ratio for biological sensing applications.[14–16] In addition, nanoporous MoS_2 membranes have been found to be excellent candidates for water desalination[17] and electric power generation.[18] As these potential applications involve MoS_2 in water environments, it is important to develop accurate MoS_2 force fields for nanofluidic applications.

Molecular dynamics (MD) simulations have been used extensively to study the performance of MoS_2 membranes in DNA sequencing,[15] water desalination,[17] osmotic power generation[18] and for a variety of other applications. However, the accuracy of MoS_2/water interfacial properties predicted by MD simulations depends on the interatomic potential employed in the simulations. Therefore, developing accurate force field parameters can result in a more quantitative estimation of MoS_2/water interfacial properties. Currently, high-accuracy force fields describing the non-bonded interaction between MoS_2 and water molecules are lacking. The force field parameters are generally developed using two approaches. First, the van der Waals (vdW) parameters are developed using the combination rule, known as the Lorentz-Berthelot[19] rule, but the accuracy of this approach is uncertain and it can lead to erroneous results.[20,21] The force field parameters (both vdW and Coulombic) can also be developed from the total interaction energy obtained from first-principles calculations where the force field interaction potential functional form is fitted to the calculated interaction energy curve.[22,23] In this approach, the accuracy of the force field parameters directly follows the fidelity of the first-principles calculations.

High-accuracy *ab initio* calculations, which can describe electron-electron correlations explicitly, are needed as the vdW interactions are affected by the correlation energy. The random phase approximation method (RPA)[24,25] treats electron-electron correlation explicitly. Prior research has shown that the parameters developed entirely from the first-principles calculations with no adjustable parameters are able to predict properties that are comparable to those of experiments.[22,23,26,27]

In this article, we use the RPA method to compute the potential energy surface between MoS_2 and water. The force field parameters are obtained from the potential energy surface and no fitting to experimental data is used in this step. Finally, the solid-liquid (MoS_2 sheet and water) work of adhesion, which is calculated by the dry-surface method[28,29] using the developed parameters, is compared with the work of adhesion values obtained from experimentally measured contact angles to validate the proposed force field parameters.

METHODOLOGY

The RPA method, which is used to treat electron-electron correlations, was first introduced by Bohm and Pines.[30–32] Later, Langreth and Perdew showed that the RPA method could be formulated using the adiabatic-connection method (AC)[33–35] along with the fluctuation-dissipation theorem (FD)[36,37] within the density functional theory (DFT).[38] This approach, known as ACFD RPA method, has been one of

[a]M. Heiranian and Y. Wu contributed equally to this work.
[b]Author to whom correspondence should be addressed: aluru@illinois.edu. URL: https://www.illinois.edu/~aluru/.

the most efficient RPA computation methods during the last decade.[39–41] The RPA correlation energy is written as

$$E_c^{\mathrm{RPA}} = \frac{1}{2\pi}\int_0^{\infty} \mathrm{Tr}\left[\mathrm{In}\left(1-\chi^0(i\omega)V\right)+\chi^0(i\omega)V\right]d\omega, \quad (1)$$

where χ^0 is the response function of the Kohn-Sham non-interacting system, V is the interacting potential operator, and ω is the frequency (see the Appendix for more information about the RPA method).

The VASP package[42,43] was used to carry out the RPA calculations. The projector-augmented wave method was applied for more efficient DFT calculations. The energy cutoff was 408 eV. An energy cutoff of up to 272 eV was used to expand the density response function in plane waves. Different MoS_2 supercell sizes and Brillouin zone sampling Monkhorst-Pack k-meshes were used for the exchange and correlation energy calculations. An 8×8 supercell with a 2×2 k-mesh and a 2×2 supercell with a 4×4 k-mesh were used for the exchange and correlation energy, respectively. The lattice constant along the direction normal to the MoS_2 surface (z-axis) was 15 Å. The RPA method is used to compute the potential energy surface between a MoS_2 cluster and a water molecule for different separation distances between the two as well as different orientations of the water molecule. The geometry of the MoS_2 and water molecule was kept rigid for simplicity. The structure of the MoS_2 cluster follows the geometry obtained from molecular statics calculations,[44] with S–S distance of 3.241 Å between two layers of sulfur atoms and a bond length of 3.17 Å, 2.42 Å, and 3.17 Å for Mo–Mo, Mo–S, and S–S, respectively.

The MD simulations have been performed using the LAMMPS package[45] to obtain the water–MoS_2 work of adhesion using the force field parameters developed in this work. Initially, a cubic box of water molecules is placed on top of a single-layer MoS_2 sheet. The water box contains 2400 water molecules. The dimension of MoS_2 sheet is about $10\ \mathrm{nm} \times 10\ \mathrm{nm}$ to ensure that the water molecules do not interact with their periodic images. The entire simulation box has a size of $10\ \mathrm{nm} \times 10\ \mathrm{nm} \times 20\ \mathrm{nm}$ in x, y, and z, respectively (the MoS_2 sheet lies in the xy plane). Both the water box and MoS_2 sheet are created using the visual molecular dynamics.[46] First, the energy of the system is minimized for 10 000 steps. Next, the system is equilibrated in the NVT ensemble for 4 ns at a pressure of 1 atm and a temperature of 300 K. The constant temperature is enforced using the Nosè-Hoover thermostat.[47,48] During the simulations, the MoS_2 atoms are kept frozen to investigate the water–MoS_2 interface properties without the effect of wall motion. A time step of 1.0 fs is used for MD integration. The short-range vdW interactions are calculated using a cutoff scheme with a cutoff distance of 1.4 nm. The long-range electrostatic interactions are calculated using the Particle-Particle-Particle-Mesh (PPPM) method.[49] During the equilibration simulation, the cubic water box spreads over the MoS_2 sheet where the energy and temperature of the system stabilize and reach constant values. The resulting configuration is used as the starting point for production simulations that are run for further 4 ns to compute the work of adhesion.

RESULTS AND DISCUSSION

Before computing the potential energy surface between MoS_2 and water, the accuracy of the calculations needs to be examined. In addition to the approximations made in the RPA mathematical formulation, other sources of error arise from the computational setup. The effect of all the sources (the incomplete basis sets, the finite lattice constant, the finite supercell, the finite k-points, and the non-zero water coverage) on the interaction energy is considered to ensure the accuracy of the calculations. First, the effect of the basis set is investigated by increasing the plane wave energy cutoff. This results in a change of about 1 meV in the energy when the energy cutoff is increased to 600 eV and 400 eV for the plane wave and the response function, respectively. Next, the lattice constant along the z-axis is increased from 15 to 20 Å in which a difference of less than 1 meV is observed in the interaction energy. The effect of k-points is studied by changing the k-grids for the exchange and correlation energies separately (see Fig. 1). As shown, the correlation energy changes with increasing the k-grid for a fixed 2×2 supercell while the exchange energy is weakly dependent on the k-grid. The correlation energy starts to converge for a 3×3 k-grid and a 2×2 supercell where increasing the k-grid to 4×4 results in a change of about 2 meV in the energy. Finally, to test the effects of the supercell size and water coverage on the energy, the supercell size is changed for the exchange energy which is shown to have a strong dependence on the size of the supercell. The exchange energy starts to converge for a 4×4 supercell and a 2×2 k-grid, while increasing the supercell size to 8×8 only improves the energy by about 2 meV. Based on the error analyses, the maximum accumulated error in the interaction energy by the RPA method is estimated to be less than 4 meV which is insignificant compared to the exchange and correlation energies.

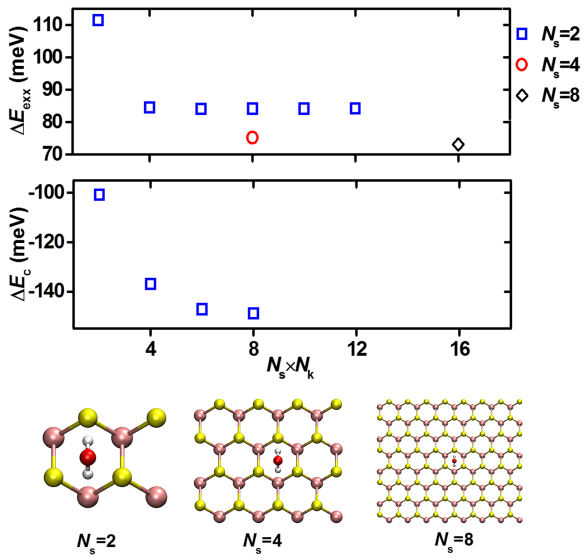

FIG. 1. The exchange energy, ΔE_{exx}, and the correlation energy, ΔE_c, between one water molecule and MoS_2 (oxygen, hydrogen, molybdenum, and sulfur atoms are shown in red, white, pink, and yellow, respectively) are shown to converge for different combinations of the $N_s \times N_s \times 1$ supercell sizes and the $N_k \times N_k \times 1$ Brillouin zone sampling Monkhorst-Pack k-meshes.

With the errors controlled, using the RPA method, the potential energy surface between MoS_2 and water is computed to implement a force field for use in MD simulations. The total interaction energy between a water molecule and a MoS_2 cluster is computed by

$$\Delta E = E_{\mathrm{MoS_2\text{-}water}} - E_{\mathrm{MoS_2}} - E_{\mathrm{water}}, \tag{2}$$

where ΔE is the total interaction energy, $E_{\mathrm{MoS_2-water}}$ is the energy of the MoS_2–water system together, and $E_{\mathrm{MoS_2}}$ and E_{water} are the energies of the MoS_2 and water molecule, respectively. These three energies are calculated separately using RPA. The partial charges for atoms of the water molecule are based on the SPC/E water model.[50] To calculate the partial charges of Mo and S atoms, the electrostatic potential of the MoS_2 (no water molecules present) is first obtained from the 2nd-order Møller-Plesset perturbation (MP2) theory calculations.[23,40] Then the partial charges are obtained by fitting to the calculated electrostatic potential.

The model used in MD simulations to describe the non-bonded interactions between the atoms of MoS_2 and water consists of two components, namely, the vdW interactions (ΔE_{vdW}) and the electrostatic interactions (ΔE_{elec}). The vdW interactions are characterized by the Lennard-Jones (LJ) potential parameters. The 12-6 LJ potential form is defined by

$$\Delta E_{\mathrm{vdW}} = \sum_{i\in \mathrm{MoS_2}} \sum_{j\in \mathrm{water}} 4\varepsilon_{ij}\left[\left(\frac{\sigma_{ij}}{r_{ij}}\right)^{12} - \left(\frac{\sigma_{ij}}{r_{ij}}\right)^{6}\right], \tag{3}$$

where ε_{ij} is the depth of the potential well between any two atoms (i and j atoms of MoS_2 and water, respectively), σ_{ij} is the distance at which the potential is zero and r_{ij} is the distance between atoms i and j. The electrostatic interactions are modeled by Coulomb's law

$$\Delta E_{\mathrm{elec}} = \sum_{i\in \mathrm{MoS_2}} \sum_{j\in \mathrm{water}} \frac{q_i q_j}{r_{ij}}, \tag{4}$$

where q_i and q_j are the partial point charges of atom i and atom j. The total interaction between the MoS_2 and water is then obtained from

$$\Delta E = \Delta E_{\mathrm{elec}} + \Delta E_{\mathrm{vdW}}. \tag{5}$$

For the vdW interactions, ε_{ij} and σ_{ij} are obtained by fitting to the RPA energies where the electrostatic component is excluded from the total energy. The water molecule has two types of atoms (O and H atoms) and MoS_2 has Mo and S atoms; therefore, four pairs of ε_{ij} and σ_{ij} parameters are required for fitting. However, for simplicity, the H–MoS_2 vdW interactions can be excluded from the parameterization fitting given the O–MoS_2 parameters can be corrected to match the potential energy from the RPA data. This simplification is valid if the vdW interaction due to O dominates compared to that of H. This is tested by plotting the vdW component energies from the RPA method for five different water orientations. As shown in Fig. 2, the energies for the five orientations are close enough to simplify the parametrization and rewrite the vdW interactions as

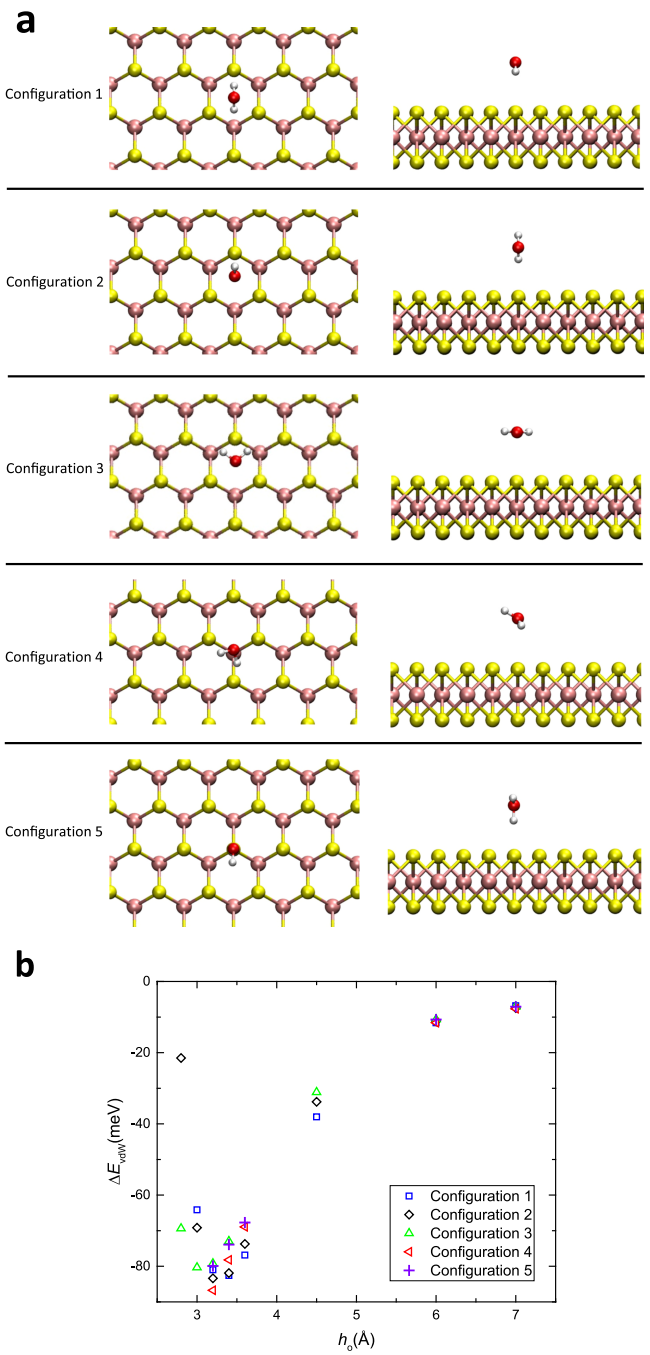

FIG. 2. (a) Schematics of the five different water configurations considered in this study. The top views and side views are presented in the left and right figures, respectively. (b) The vdW interaction energies between MoS_2 and water for the five different water orientations as a function of their separation distance (h_o), which is the shortest distance between the water oxygen atom and the plane of the sulfur atoms facing the water molecule. The unit cells and k-meshes of ($N_s = 8$ and $N_k = 2$) and ($N_s = 2$ and $N_k = 4$) are used for the calculations of the exchange and correlation energies, respectively.

$$\Delta E_{\mathrm{vdW}} = \sum_{i\in \mathrm{MoS_2}} 4\varepsilon_{i\mathrm{O}}\left[\left(\frac{\sigma_{i\mathrm{O}}}{r_{i\mathrm{O}}}\right)^{12} - \left(\frac{\sigma_{i\mathrm{O}}}{r_{i\mathrm{O}}}\right)^{6}\right]. \tag{6}$$

The Boltzmann averaged vdW interaction energies for the five different water orientations (Fig. 2) are fitted, using the

TABLE I. Summary of water–MoS_2 force field parameters in the literature as well as the parameters developed in this work. The Lennard-Jones parameters σ_{Mo-O}, σ_{S-O}, ε_{Mo-O}, and ε_{S-O} and the partial charges q_{Mo} and q_S are tabulated for each force field. The partial charges of water are taken based on the water model used. σ_{Mo-O} and σ_{S-O} are in Å, ε_{Mo-O} and ε_{S-O} are in kcal/mol, and the charges are represented in the unit of the elementary charge.

Reference	MoS_2–water model	σ_{Mo-O}	ε_{Mo-O}	σ_{S-O}	ε_{S-O}	q_{Mo}/q_S
Becker *et al.*[58]	Combine Mo–Mo, S–S from Becker *et al.*[58] and O–O from SPC/E[50]	2.876	3.1447	2.920	1.4615	0.70/–0.35
Morita *et al.*[59]	Combine Mo–Mo, S–S from Morita *et al.*[59] and O–O from SPC/E[50]	2.858	1.7327	3.268	0.0814	0.76/–0.38
Varshney *et al.*[60]	Combine Mo–Mo, S–S from Varshney *et al.*[60] and O–O from SPC/E[50]	2.858	1.7327	3.268	0.4659	0.76/–0.38
Farimani *et al.*[15]	Combine Mo–Mo, S–S from Stewart[44] and O–O from TIP3P[61]	3.683	0.0458	3.148	0.2228	0.00/0.00
Heiranian *et al.*[17]	Combine Mo–Mo, S–S from Liang *et al.*[62,63] and O–O from SPC/E[50]	3.683	0.0458	3.148	0.2677	0.00/0.00
Luan and Zhou[64]	Combine Mo–Mo, S–S from Luan and Zhou[64] and O–O from SPC/E[50]	2.858	0.1421	3.333	0.1971	0.76/–0.38
This work	Fit to RPA data	3.934	0.0458	3.362	0.2680	0.60/–0.30

least-squares method, to the potential function in Eq. (6) to obtain the vdW parameters. The vdW parameters from the fitting are tabulated in Table I. Also included in the table are the parameters obtained from the combination rule used in the literature. In addition, the water models and partial charges on Mo and S atoms used in each work are summarized in the table. In order to validate the accuracy of the proposed parameters, MD simulations can be used to predict properties of water–MoS_2 interface which are then compared with those of experimental measurements.

The contact angle of water on MoS_2 surfaces is one of the water–MoS_2 properties reported by several experimental measurements.[51–56] Most of the experimental contact angles lie in the range of 65°–75°. The variations in these experimental values are possibly due to the susceptibility of MoS_2 to surface contaminations.[51,52] However, the droplet sizes, simulated in MD, are of nanometers, which are much smaller than the macroscopic droplets used in experiments. The contact angle values, θ, from simulations, which are extrapolated using the modified Young's equation, are a function of the liquid-vapor surface tension of the water droplet, γ_{LV}. But this may not be an accurate extrapolation since γ_{LV} itself changes with the droplet size at the nanoscale. In addition, water models, in MD simulations, result in γ_{LV} values that are different from the experimental value. It has been shown that these differences can significantly affect the θ estimation in MD leading to possibly unreliable comparison with the experimental contact angles.[29] Alternatively, the solid-liquid work of adhesion, W_{SL}, is a recommended interface property to validate force field parameters against the experimental data as it is shown to be independent of water models and can be calculated explicitly in MD with no dependence on γ_{LV} and θ.[28,29]

The work of adhesion is obtained explicitly using the dry-surface in MD simulations.[28] The work of adhesion is the work per unit area of the solid-liquid interface required to isolate the liquid droplet from the solid surface such that there is no interaction between the liquid and solid. In the dry-surface method, this is achieved by varying the interaction parameters (ε and q) from the actual interactive state (A) to a state (B) in which the interaction energy per unit area between the surface and liquid is insignificant relative to the work of adhesion. The work of adhesion for the system of a water droplet and MoS_2 surface is obtained from the following integrations:

$$W_{SL} = \frac{1}{a}\left[\int_{\varepsilon_A^{Mo-O}}^{\varepsilon_B^{Mo-O}} \left\langle \frac{\partial U_{LJ}^{Mo-O}}{\partial \varepsilon} \right\rangle d\varepsilon + \int_{\varepsilon_A^{S-O}}^{\varepsilon_B^{S-O}} \left\langle \frac{\partial U_{LJ}^{S-O}}{\partial \varepsilon} \right\rangle d\varepsilon + \int_{q_A^{Mo}}^{q_B^{Mo}} \left\langle \frac{\partial U_{elec}^{Mo-water}}{\partial q} \right\rangle dq + \int_{q_A^{S}}^{q_B^{S}} \left\langle \frac{\partial U_{elec}^{S-water}}{\partial q} \right\rangle dq \right], \quad (7)$$

where a is the surface area of the MoS_2 membrane, and U_{LJ}^{n-m} and U_{elec}^{n-m} are the interaction energies between atoms of type n and m due to the LJ and Coulombic interactions, respectively. For the force fields with no partial charges, the last two integrals are ignored. The differentiation and integration are performed numerically using the second-order accurate finite difference method and trapezoidal rule. For experiments, W_{SL} is obtained from the Young-Dupré equation

$$W_{SL} = \gamma_{LV}(1 + \cos(\theta)), \quad (8)$$

where the experimental values of γ_{LV} and θ are used to calculate the work of adhesion. The work of adhesion values for different force fields in MD simulations as well as the experimental values as a function of the binding energy are

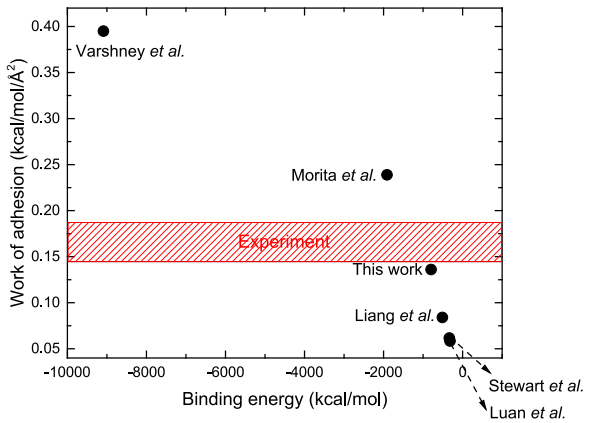

FIG. 3. The solid-liquid work of adhesion simulated by MD for the force field parameters in the literature, and from this work as a function of the binding energy between water and MoS_2. For Becker *et al.*,[58] the work of adhesion and binding energy (not shown for better presentation of other data points) are 0.945 (kcal/mol)/Å^2 and −25 768.29 kcal/mol, respectively.

shown in Fig. 3. As shown, the parameters developed in this work, using the RPA energies, lead to a work of adhesion value which is closest to the range of work of adhesion values obtained from the experimental contact angle measurements. Note that no fitting from experimental data has been applied to develop the force field. The agreement with experimental data shows that using *ab initio* calculations directly is a reasonably rigorous method to develop accurate force field parameters without any fit to experiments. This has been shown consistently in our other force field developments for graphitic-carbon-water interaction[22] and hexagonal boron-nitride-water interactions.[23,40]

CONCLUSION

In summary, we use the ACDF RPA method to calculate the interaction energy between MoS_2 and water. The RPA results, without any fitting to the experimental data, are used to develop force field parameters that are subsequently used in MD simulations. The corresponding water–MoS_2 work of adhesion in MD simulations is found to be comparable to the work of adhesion obtained from the experimental contact angle measurements. The good agreement with experiments shows that developing force field parameters directly from first-principle calculations is an accurate method to predict properties of emerging systems at molecular scales.

ACKNOWLEDGMENTS

This work is supported by AFOSR under Grant No. FA9550-12-1-0464 and by NSF under Grant Nos. 1264282, 1420882, 1506619, and 1545907. This work used the Extreme Science and Engineering Discovery Environment (XSEDE) which is supported by National Science Foundation Grant No. OCI-1053575. This research is part of the Blue Waters sustained-petascale computing project, which is supported by the National Science Foundation (Award Nos. OCI0725070 and ACI-1238993) and the state of Illinois. Blue Waters is a joint effort of the University of Illinois at Urbana-Champaign and its National Center for Supercomputing Applications.

APPENDIX: RPA METHOD

For a given electronic system, the total energy (E) of the ground state, in the Kohn-Sham (KS) DFT, is written as

$$E = T_{\mathrm{KS}} + E_{\text{ion-e}} + E_{\mathrm{H}} + E_{\mathrm{xc}}, \tag{A1}$$

where T_{KS} is the kinetic energy of the KS non-interacting system, $E_{\text{ion-e}}$ is the ion-electron interaction energy, E_{H} is the Hartree energy, and E_{xc} is the electron-electron interaction energy known as the exchange-correlation energy. The GGA-PBE functional[57] is used to obtain the electron density based on the single-particle KS orbitals. All the terms in Eq. (A1) are functionals of the electron density, $\rho(\mathbf{r})$, which, in the KS DFT, is obtained by

$$\rho(\mathbf{r}) = \sum_{i}^{N} |\phi_i(\mathbf{r})|^2, \tag{A2}$$

where N is the number of particles and $\phi_i(\mathbf{r})$ is the KS orbital for a single particle i. In this approach, the difficulty arises in computing the electron-electron interaction term (E_{xc}). To do that, the AC formulation is first used to write the ground state total energy of the system. The Hamiltonian of the system ($\hat{H}$) can be written as a summation of non-perturbative ($\lambda = 0$) and perturbative (λ) terms as follows:

$$\hat{H} = \hat{H}_0 + \lambda \hat{H}_1, \tag{A3}$$

where λ is a dimensionless parameter ($0 \le \lambda \le 1$). Considering the Hamiltonian for an electronic system and that $H|\Psi_\lambda\rangle = E|\Psi_\lambda\rangle$ (Ψ_λ is the wave function of the ground state), the total energy in the ground state is obtained by

$$E = \langle\Psi_0|\hat{H}_0|\Psi_0\rangle + \int_0^1 \langle\Psi_\lambda|\left[\hat{H}_1 + \lambda\frac{d\hat{H}_1}{d\lambda}\right]|\Psi_\lambda\rangle\, d\lambda. \tag{A4}$$

In KS DFT, the electron density is kept fixed and the zeroth order ground state wave function, $|\Psi_0\rangle$, is simply the Slater determinant of the single-electron orbitals. Given that the electron-electron interaction operator is defined as $V = \sum_{i,j\neq i}^{N} \frac{\lambda}{|\mathbf{r}_i - \mathbf{r}_j|}$ ($\mathbf{r}_i$ is position vector of electron i), by equating equations (A1) and (A4), the exchange-correlation energy is written as

$$E_{\mathrm{xc}} = \frac{1}{2}\int_0^1 \left[\iint \frac{\left(\langle\Psi_\lambda|\,\delta\hat{\rho}(\mathbf{r})\,\delta\hat{\rho}(\mathbf{r}')\,|\Psi_\lambda\rangle - \delta(\mathbf{r}-\mathbf{r}')\,\rho(\mathbf{r})\right)}{|\mathbf{r}-\mathbf{r}'|} d\mathbf{r}d\mathbf{r}'\right] d\lambda, \tag{A5}$$

where $\hat{\rho}(\mathbf{r}) = \sum_{i=1}^{N} \delta(\mathbf{r}-\mathbf{r}_i)$ is the electron-density operator, $\delta\hat{\rho}(\mathbf{r}) = \hat{\rho}(\mathbf{r}) - \rho(\mathbf{r})$ is the density fluctuation operator, and $\rho(\mathbf{r})$ is the expectation value of the electron-density operator.

The zero-temperature fluctuation-dissipation theorem is used to express the expectation value of the two-particle density fluctuation operator in Eq. (A5) as a frequency integration of the dissipation of the system

$$\langle\Psi_\lambda|\,\delta\hat{\rho}(\mathbf{r})\,\delta\hat{\rho}(\mathbf{r}')\,|\Psi_\lambda\rangle = -\frac{1}{\pi}\int_0^\infty \mathrm{Im}\,\chi^\lambda(\omega,\mathbf{r},\mathbf{r}')d\omega, \tag{A6}$$

where $\chi^\lambda(\omega,\mathbf{r},\mathbf{r}')$ is the linear density-density response function of the interacting system which can be expressed in terms

of the response function of the KS non-interacting system, $\chi^0(\omega, \mathbf{r}, \mathbf{r}')$, as follows:[39]

$$\chi^{\lambda}(i\omega, \mathbf{r}, \mathbf{r}') = \chi^{0}(i\omega, \mathbf{r}, \mathbf{r}') + \iint \chi^{0}(i\omega, \mathbf{r}, \mathbf{r}_1)\left(V(\mathbf{r}_1 - \mathbf{r}_2) + f_{\mathrm{xc}}^{\lambda}(i\omega, \mathbf{r}_1, \mathbf{r}_2)\right)\chi^{\lambda}(\omega, \mathbf{r}_2, \mathbf{r}')\, d\mathbf{r}_1 d\mathbf{r}_2, \quad \text{(A7)}$$

where V is the interacting potential operator and $f_{\mathrm{xc}}^{\lambda}$ is the exchange-correlation kernel. $\chi^0(\omega, \mathbf{r}, \mathbf{r}')$ is simply obtained by the knowledge of the single-particle KS orbitals. In order to perform the integration in Eq. (A6) practically, the response function, given in Eq. (A7), needs to be approximated by neglecting $f_{\mathrm{xc}}^{\lambda}$. This approximation is known as the random phase approximation [we write the approximated response function as $\chi_{\mathrm{RPA}}^{\lambda}(\omega, \mathbf{r}, \mathbf{r}')$]. Using Eqs. (A5)–(A7), the exchange-correlation energy (E_{xc}) is given by

$$E_{\mathrm{xc}} = \left\{-\frac{1}{2\pi}\iint\left[\frac{1}{|\mathbf{r}-\mathbf{r}'|}\int_0^{\infty}\left(\chi^{0}(i\omega, \mathbf{r}, \mathbf{r}') - \delta(\mathbf{r}-\mathbf{r}')\,\rho(\mathbf{r})\right)d\omega\right]d\mathbf{r}d\mathbf{r}'\right\} + \left\{-\frac{1}{2\pi}\iint\left[\frac{1}{|\mathbf{r}-\mathbf{r}'|}\int_0^{\infty}\left(\int_0^{1}\left(\chi_{\mathrm{RPA}}^{\lambda}(i\omega, \mathbf{r}, \mathbf{r}') - \chi^{0}(i\omega, \mathbf{r}, \mathbf{r}')\right)d\lambda\right)d\omega\right]d\mathbf{r}d\mathbf{r}'\right\}, \quad \text{(A8)}$$

where the first and second terms in $\{\}$ are the exchange energy (E_{x}) and RPA correlation energy ($E_{\mathrm{c}}^{\mathrm{RPA}}$), respectively. The RPA correlation energy can be written in the following reduced form:

$$E_{\mathrm{c}}^{\mathrm{RPA}} = \frac{1}{2\pi}\int_0^{\infty}\mathrm{Tr}\left[\mathrm{In}\left(1 - \chi^{0}(i\omega)\,V\right) + \chi^{0}(i\omega)\,V\right]d\omega. \quad \text{(A9)}$$

[1] K. Koga, G. T. Gao, H. Tanaka, and X. C. Zeng, "Formation of ordered ice nanotubes inside carbon nanotubes," Nature **412**, 802–805 (2001).
[2] R. J. Mashl, S. Joseph, N. R. Aluru, and E. Jakobsson, "Anomalously immobilized water: A new water phase induced by confinement in nanotubes," Nano Lett. **3**, 589–592 (2003).
[3] M. Majumder, N. Chopra, R. Andrews, and B. J. Hinds, "Nanoscale hydrodynamics: Enhanced flow in carbon nanotubes," Nature **438**, 44 (2005).
[4] J. K. Holt *et al.*, "Fast mass transport through sub-2-nanometer carbon nanotubes," Science **312**, 1034–1037 (2006).
[5] S. Joseph and N. R. Aluru, "Why are carbon nanotubes fast transporters of water?," Nano Lett. **8**, 452–458 (2008).
[6] K. Falk, F. Sedlmeier, L. Joly, R. R. Netz, and L. Bocquet, "Molecular origin of fast water transport in carbon nanotube membranes: Superlubricity versus curvature dependent friction," Nano Lett. **10**, 4067–4073 (2010).
[7] A. B. Farimani, M. Heiranian, and N. R. Aluru, "Nano-electro-mechanical pump: Giant pumping of water in carbon nanotubes," Sci. Rep. **6**, 26211 (2016).
[8] S. Joseph and N. R. Aluru, "Pumping of confined water in carbon nanotubes by rotation-translation coupling," Phys. Rev. Lett. **101**, 064502 (2008).
[9] K. Kurotobi and Y. Murata, "A single molecule of water encapsulated in fullerene C_{60}," Science **333**, 613–616 (2011).
[10] A. B. Farimani, Y. Wu, and N. R. Aluru, "Rotational motion of a single water molecule in a buckyball," Phys. Chem. Chem. Phys. **15**, 17993–18000 (2013).
[11] M. E. Suk and N. R. Aluru, "Water transport through ultrathin graphene," J. Phys. Chem. Lett. **1**, 1590–1594 (2010).
[12] E. N. Wang and R. Karnik, "Water desalination graphene cleans up water," Nat. Nanotechnol. **7**, 552–554 (2012).
[13] R. C. Rollings, A. T. Kuan, and J. A. Golovchenko, "Ion selectivity of graphene nanopores," Nat. Commun. **7**, 7 (2016).
[14] K. Liu, J. D. Feng, A. Kis, and A. Radenovic, "Atomically thin molybdenum disulfide nanopores with high sensitivity for DNA translocation," ACS Nano **8**, 2504–2511 (2014).
[15] A. B. Farimani, K. Min, and N. R. Aluru, "DNA base detection using a single-layer MoS_2," ACS Nano **8**, 7914–7922 (2014).
[16] J. D. Feng *et al.*, "Identification of single nucleotides in MoS_2 nanopores," Nat. Nanotechnol. **10**, 1070 (2015).
[17] M. Heiranian, A. B. Farimani, and N. R. Aluru, "Water desalination with a single-layer MoS_2 nanopore," Nat. Commun. **6**, 8616 (2015).
[18] J. D. Feng *et al.*, "Single-layer MoS_2 nanopores as nanopower generators," Nature **536**, 197 (2016).
[19] S. I. Sandler and J. K. Wheatley, "Intermolecular potential parameter combining rules for Lennard-Jones 6-12 potential," Chem. Phys. Lett. **10**, 375 (1971).
[20] J. Delhommelle and P. Millie, "Inadequacy of the Lorentz-Berthelot combining rules for accurate predictions of equilibrium properties by molecular simulation," Mol. Phys. **99**, 619–625 (2001).
[21] D. Boda and D. Henderson, "The effects of deviations from Lorentz-Berthelot rules on the properties of a simple mixture," Mol. Phys. **106**, 2367–2370 (2008).
[22] Y. B. Wu and N. R. Aluru, "Graphitic carbon-water nonbonded interaction parameters," J. Phys. Chem. B **117**, 8802–8813 (2013).
[23] Y. B. Wu, L. K. Wagner, and N. R. Aluru, "The interaction between hexagonal boron nitride and water from first principles," J. Chem. Phys. **142**, 234702 (2015).
[24] J. Harl and G. Kresse, "Accurate bulk properties from approximate many-body techniques," Phys. Rev. Lett. **103**, 056401 (2009).
[25] S. Lebègue *et al.*, "Cohesive properties and asymptotics of the dispersion interaction in graphite by the random phase approximation," Phys. Rev. Lett. **105**, 196401 (2010).
[26] T. A. Hilder *et al.*, "Validity of current force fields for simulations on boron nitride nanotubes," Micro Nano Lett. **5**, 150–156 (2010).
[27] H. Li and X. C. Zeng, "Wetting and interfacial properties of water nanodroplets in contact with graphene and monolayer boron-nitride sheets," ACS Nano **6**, 2401–2409 (2012).
[28] F. Leroy and F. Müller-Plathe, "Dry-surface simulation method for the determination of the work of adhesion of solid-liquid interfaces," Langmuir **31**, 8335–8345 (2015).
[29] F. Leroy, S. Y. Liu, and J. G. Zhang, "Parametrizing nonbonded interactions from wetting experiments via the work of adhesion: Example of water on graphene surfaces," J. Phys. Chem. C **119**, 28470–28481 (2015).
[30] D. Bohm and D. A. Pines, "Collective description of electron interactions. I. Magnetic interactions," Phys. Rev. **82**, 625–634 (1951).
[31] D. Bohm and D. A. Pines, "Collective description of electron interactions: III. Coulomb interactions in a degenerate electron gas," Phys. Rev. **92**, 609–625 (1953).
[32] D. Pines and D. A. Bohm, "Collective description of electron interactions: II. Collective vs individual particle aspects of the interactions," Phys. Rev. **85**, 338–353 (1952).
[33] D. C. Langreth and J. P. Perdew, "Exchange-correlation energy of a metallic surface: Wave-vector analysis," Phys. Rev. B **15**, 2884–2901 (1977).
[34] D. C. Langreth and J. P. Perdew, "Exchange-correlation energy of a metallic surface: Wave-vector analysis. II," Phys. Rev. B **26**, 2810–2818 (1982).
[35] O. Gunnarsson, M. Jonson, and B. I. Lundqvist, "Exchange and correlation in atoms, molecules and solids," Phys. Lett. A **59**, 177–179 (1976).

[36]H. B. Callen and R. F. Greene, "On a theorem of irreversible thermodynamics," Phys. Rev. **86**, 702–710 (1952).
[37]R. F. Greene and H. B. Callen, "On the formalism of thermodynamic fluctuation theory," Phys. Rev. **83**, 1231–1235 (1951).
[38]P. Hohenberg and W. Kohn, "Inhomogeneous electron gas," Phys. Rev. B **136**, B864 (1964).
[39]X. G. Ren, P. Rinke, C. Joas, and M. Scheffler, "Random-phase approximation and its applications in computational chemistry and materials science," J. Mater. Sci. **47**, 7447–7471 (2012).
[40]Y. B. Wu, L. K. Wagner, and N. R. Aluru, "Hexagonal boron nitride and water interaction parameters," J. Chem. Phys. **144**, 164118 (2016).
[41]H. Eshuis, J. E. Bates, and F. Furche, "Electron correlation methods based on the random phase approximation," Theor. Chem. Acc. **131**, 1084 (2012).
[42]G. Kresse and J. Furthmüller, "Efficiency of *ab-initio* total energy calculations for metals and semiconductors using a plane-wave basis set," Comput. Mater. Sci. **6**, 15–50 (1996).
[43]G. Kresse and J. Hafner, "*Ab initio* molecular-dynamics for open-shell transition-metals," Phys. Rev. B **48**, 13115–13118 (1993).
[44]J. A. Stewart and D. E. Spearot, "Atomistic simulations of nanoindentation on the basal plane of crystalline molybdenum disulfide (MoS_2)," Modell. Simul. Mater. Sci. Eng. **21**, 045003 (2013).
[45]S. Plimpton, "Fast parallel algorithms for short-range molecular-dynamics," J. Comput. Phys. **117**, 1–19 (1995).
[46]W. Humphrey, A. Dalke, and K. Schulten, "VMD: Visual molecular dynamics," J. Mol. Graphics Modell. **14**, 33–38 (1996).
[47]W. G. Hoover, "Canonical dynamics: Equilibrium phase-space distributions," Phys. Rev. A **31**, 1695–1697 (1985).
[48]S. A. Nose, "Unified formulation of the constant temperature molecular-dynamics methods," J. Chem. Phys. **81**, 511–519 (1984).
[49]O. Buneman, "Computer-simulation using particles (R. W. Hockney and J. W. Eastwood)," SIAM Rev. **25**, 425–426 (1983).
[50]H. J. C. Berendsen, J. R. Grigera, and T. P. Straatsma, "The missing term in effective pair potentials," J. Phys. Chem. **91**, 6269–6271 (1987).
[51]A. Kozbial, X. Gong, H. T. Liu, and L. Li, "Understanding the intrinsic water wettability of molybdenum disulfide (MoS_2)," Langmuir **31**, 8429–8435 (2015).
[52]P. K. Chow *et al.*, "Wetting of mono and few-layered WS_2 and MoS_2 films supported on Si/SiO_2 substrates," ACS Nano **9**, 3023–3031 (2015).
[53]A. P. S. Gaur *et al.*, "Surface energy engineering for tunable wettability through controlled synthesis of MoS_2," Nano Lett. **14**, 4314–4321 (2014).
[54]P. Navabpour, D. G. Teer, D. J. Hitt, and M. Gilbert, "Evaluation of non-stick properties of magnetron-sputtered coatings for moulds used for the processing of polymers," Surf. Coat. Technol. **201**, 3802–3809 (2006).
[55]S. Zhang, X. T. Zeng, Z. G. Tang, and M. J. Tan, "Exploring the antisticking properties of solid lubricant thin films in transfer molding," Int. J. Mod. Phys. B **16**, 1080–1085 (2002).
[56]U. Halim *et al.*, "A rational design of cosolvent exfoliation of layered materials by directly probing liquid-solid interaction," Nat. Commun. **4**, 2213 (2013).
[57]J. P. Perdew, K. Burke, and M. Ernzerhof, "Generalized gradient approximation made simple," Phys. Rev. Lett. **77**, 3865–3868 (1996).
[58]U. Becker, K. M. Rosso, R. Weaver, M. Warren, and M. F. Hochella, "Metal island growth and dynamics on molybdenite surfaces," Geochim. Cosmochim. Acta **67**, 923–934 (2003).
[59]Y. Morita *et al.*, "Development of a new molecular dynamics method for tribochemical reaction and its application to formation dynamics of MoS_2 tribofilm," Appl. Surf. Sci. **254**, 7618–7621 (2008).
[60]V. Varshney *et al.*, "MD simulations of molybdenum disulphide (MoS_2): Force-field parameterization and thermal transport behavior," Comput. Mater. Sci. **48**, 101–108 (2010).
[61]W. L. Jorgensen, J. Chandrasekhar, J. D. Madura, R. W. Impey, and M. L. Klein, "Comparison of simple potential functions for simulating liquid water," J. Chem. Phys. **79**, 926–935 (1983).
[62]T. Liang, S. R. Phillpot, and S. B. Sinnott, "Erratum: Parametrization of a reactive many-body potential for Mo–S systems [Phys. Rev. B 79, 245110 (2009)]," Phys. Rev. B **85**, 199903 (2012).
[63]T. Liang, S. R. Phillpot, and S. B. Sinnott, "Parametrization of a reactive many-body potential for Mo–S systems," Phys. Rev. B **79**, 245110 (2009).
[64]B. Q. Luan and R. H. Zhou, "Wettability and friction of water on a MoS_2 nanosheet," Appl. Phys. Lett. **108**, 5 (2016).